Geochemistry of the Timberville Zn-Pb District, Rockingham County, VA.

Tyler Newton GEOL 394H April 26th, 2013

Advisors:

Dr. Philip Candela Dr. Philip Piccoli Dr. William McDonough

Abstract

The Timberville Zn-Pb district comprises on the order of 10 sulfide deposits in the Shenandoah Valley of the Appalachians. Sphalerite is common to all locations, but pyrite, galena, fluorite, and chalcopyrite are reported to occur in varying amounts. Appold et al. (1995) suggested, based on sulfur isotope compositions of samples within the district, that sulfide mineralization occurred in two different stages. The presence of zoned sphalerite in at least one location in the Timberville Zn-Pb district is consistent with multiple stages of mineralization. I hypothesize that the salinity of fluid inclusions in sphalerite can be correlated to chemical composition of the host sphalerite. I have tested my hypothesis by analyzing multiple samples of sphalerite from several deposits within the Timberville Zn-Pb district with an electron probe microanalyzer and a laser ablation inductively coupled plasma mass spectrometer. Additionally, I have performed fluid inclusion microthermometric freezing experiments on grains of sphalerite from the Timberville Zn-Pb district. The concentrations of iron and gallium in sphalerite grains from the Bowers-Campbell mine and the Weatherholz mine are correlative with the salinity of fluid inclusions in the host sphalerite. Sphalerite with a higher concentration of iron, and therefore a darker color, hosts fluid inclusions with a lower freezing point depression than sphalerite with a lower Fe concentration. The relationship of the concentration of gallium with respect to salinity is conversely proportional to that of iron. A correlation between fluid inclusion salinity and the chemical composition of the host sphalerite may suggest that the degree of mixing of formational fluids produces the observed variations in FI salinity and the chemical composition of the host sphalerite.

Table of Contents

Abstract	1
Introduction	3
Sediment-hosted Pb-Zn Deposits	
Appalachian Mississippi Valley-Type Deposits	4
Geologic Setting	5
Objectives	6
Hypothesis	6
Test of Hypotheses	6
Methods	7
Samples	
Sample Preparation	
Fluid Inclusion Microthermometry	
Mineral Analyses Element Selection	
Electron Probe Microanalyzer	
Laser Ablation Inductively Coupled Plasma Mass Spectrometry (LA-ICPMS)	
Error Analysis	
Results	12
Petrography	
Fluid Inclusion Microthermometry Results	
Electron Probe Microanalyzer Results	
Laser Ablation Inductively Coupled Plasma Mass Spectrometry Results	14
Discussion	16
Chemical Variation in Sphalerite	16
Fluid Inclusion Freezing Point Depressions in Sphalerite	
Implications For Formational Fluids	17
Suggestions For Future Work	18
Conclusions	18
Acknowledgements	18
Bibliography	19
Appendix A	22
Appendix B	
Appendix C	

Introduction

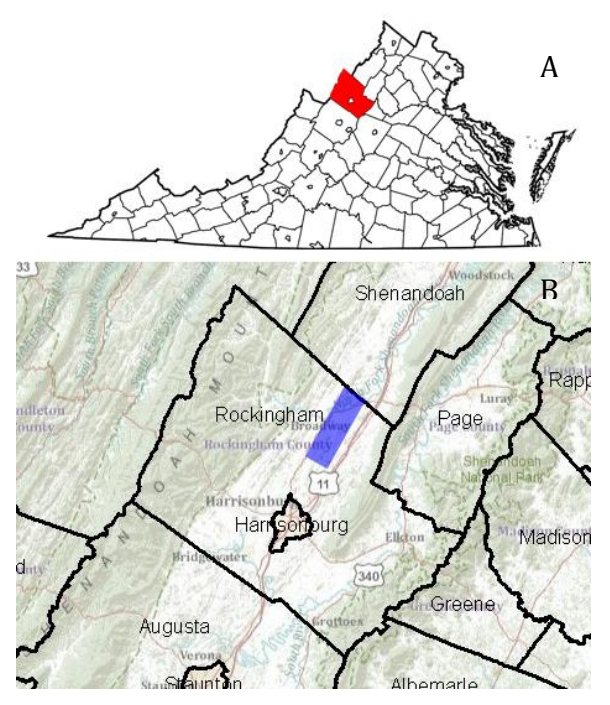


Figure 1: A) Map of Virginia, USA. Rockingham County is highlighted in red. B) The Timberville district in Rockingham County is highlighted in blue.

The Timberville Zn-Pb district, located in Rockingham County, VA, contains about 10 deposits of carbonate sediment-hosted sulfide mineralization. The district is approximately 30 km by 15 km and located in the Great Valley Region of the Appalachians in the Eastern United States (Figure 1). Two deposits within the district, the Bowers-Campbell mine and the Weatherholz mine, were exploited for their sulfide minerals, while the remaining deposits have either been prospected, or only briefly described in previous works (Herbert and Young, 1956, Sweet et al., 1989). The primary sulfide mineral present in the Timberville district is sphalerite (ZnS), followed by pyrite (FeS₂), and minor occurrences of galena (PbS),

chalcopyrite (CuFeS₂), and fluorite (CaF₂) (Herbert and Young, 1956). Sulfide mineralization is strata-bound in the Upper Beekmantown dolomite, which is

interpreted to be a paleokarst breccia in the Timberville district (Hoagland, 1971). As a result of the high permeability of the paleokarsts, sphalerite and other sulfides were largely deposited in open spaces, with less than 15% of sulfide mineralization occurring as host rock replacement (Hoagland, 1971). Gangue hydrothermal dolomite fills the remaining space in the paleokarst network that is not occupied by host rock or sulfides. Sulfide mineralization in the Timberville Zn-Pb district is thought to occur after brecciation of the host rock, and it has been suggested that sulfide mineralization occurred in two different stages, based on sulfur isotope compositions of samples within the district (Appold et al., 1995).

Sediment-hosted Pb-Zn Deposits

The Timberville Zn-Pb district is classified as a Mississippi Valley-Type (MVT) deposit in multiple studies (Appold et al., 1995; Kesler and van der Pluijm, 1990; Kesler et al., 1994; Leach and Rowan, 1986; Leach et al., 2010). MVT deposits are a subtype of sediment-hosted Pb-Zn deposits, which are the largest lead and zinc resources on Earth (Leach et al., 2005). The two main types of sediment-hosted Pb-Zn deposits are MVT and sedimentary exhalative (SEDEX) deposits. SEDEX deposits are classified on the basis of the presence of laminated sulfides that are parallel to bedding, typically in shale, siltstone, or chert units (Leach et al., 2005). MVT deposits are hosted in platform carbonate sequences that were deposited in shallow water (Leach et al., 2010). The

distinction between MVT and SEDEX deposits can be subjective, as some MVT deposits display laminated ore textures, whereas some SEDEX ores replace carbonates. Irish-Type carbonate-hosted Pb-Zn deposits are another variant of sediment-hosted Pb-Zn deposits. Irish-Type deposits are typically wedge shaped, and they contain sulfide lenses that are typically fault-controlled (Leach et al., 2005). A review of the characteristics of MVT deposits follows.

MVT deposits are epigenetic, are hosted dominantly in carbonates, and are not associated with igneous activity. They typically occur in districts, which are a collection of genetically related deposits that range in size from 1000 km² to 10000 km² (Leach et al., 2010). Most MVT deposits are small, in the range of 1 to 10 million metric tons of ore, but they can be as large as 80 million metric tons, with grade up to 6.5% Zn, and 3% Pb. MVT deposits range in age from Proterozoic to Tertiary (Alldrick and Sangster, 2005). The host carbonate rocks of MVT deposits form in shallow water in tidal and subtidal marine environments (Alldrick and Sangster, 2005), and most commonly include dolostone, limestone, or partially dolomitized limestone. The most common host rock alteration found associated with MVT deposits is dolomitization. Dissolution and brecciation are also found. Silicification of host rocks is minor, and MVT deposits commonly occur in paleokarst networks (Leach et al., 2010). The mechanism of ore deposit formation is thought to be the movement of brines into the hosting structure by compaction-driven fluid flow or gravity-driven fluid flow (Alldrick and Sangster, 2005). MVT ores form at low-temperatures, in the range of 75 °C to 200 °C (Leach et al., 2005). The ore-forming fluids appear to be ultimately derived from evaporated seawater, comparable to oil field brines. A common paragenesis sequence, or order of precipitation of the minerals, for MVT deposits is pyrite \Rightarrow sphalerite \Rightarrow galena (Alldrick and Sangster, 2005). Sphalerite, which occurs commonly as a cement in the collapse breccia, can display compositional, and associated color banding. Some MVT districts display metal zoning, showing a decrease in iron with increasing distance from the area of most intense sulfide mineralization (Alldrick and Sangster, 2005, Marie et al., 2001). MVT deposits can be highly irregular in form, and different MVT deposits can vary in many of the above listed properties.

Appalachian Mississippi Valley-Type Deposits

The MVT deposits that occur in the Appalachians are referred to as Appalachian MVT deposits (Appold et al., 1995); many are in the Valley and Ridge Province. The Ordovician-hosted MVT deposits in the Appalachian orogen are limited to the shelf carbonate sequence, known as the Beekmantown Group in northern Virginia, Maryland, and Pennsylvania, the Knox Group in Alabama, Georgia, Tennessee and southern Virginia, and the Port-au-Port and St. George Groups in Newfoundland (Hoagland, 1971). Also, the ore mineralization at each deposit is associated with paleokarst breccias. Sphalerite in these deposits is reported as being anomalously low in iron, and enriched in cadmium (Kesler and van der Pluijm, 1990). Galena and chalcopyrite are rare in Appalachian MVT deposits, and barite and fluorite are only present in distinct districts (Kesler and van der Pluijm, 1990). Hence, these deposits have Zn/Pb ratios that are higher than MVT deposits elsewhere. It is hypothesized that mineralization occurred in these deposits during the Alleghanian orogeny (Leach and Rowan, 1986). Kesler and van der Pluijm (1990) list the Appalachian MVT districts as the Sweetwater, Masscot-

Jefferson City, Copper Ridge, Fall Branch, Marion, Timberville, Friendsville, Central Pennsylvanian, Newfoundland, and Austinville-Ivanhoe districts.

Geologic Setting

The Timberville Zn-Pb district is located in Rockingham County, VA, which borders West Virginia and the city of Harrisonburg, VA. The Timberville district is in the Shenandoah Valley and is adjacent to Massanutten Mountain, which is a dominant topographic and structural feature to the east. The Allegheny Mountains are to the west of the Timberville district. Triassic and Eocene intrusive rocks of mostly basaltic and andesitic composition also occur in the southernmost part of the Timberville district (Johnson, 1971). The Appalachian Valley and Ridge consists of Cambrian to Lower Permian sedimentary rocks that were thrust in the northwest direction over the North American craton (Appold et al., 1995). The Appalachian province is bordered on the northwest by gently folded, middle to upper Paleozoic rocks of the Appalachian plateau (Appold et al., 1995). In the southeast, Precambrian metamorphic rocks of the Blue Ridge border the Appalachian Valley and Ridge. Paleozoic metamorphic rocks define the northeastern boundary of the Valley and Ridge.

Sulfide mineralization in the Timberville Zn-Pb district occurs in the upper Beekmantown dolomite. In this area, the Beekmantown Formation is about 760 m thick, and is predominantly dolomite with interbedded limestone in the upper 100 meters (Herbert and Young, 1956), with chert horizons present near the middle of the unit. The Beekmantown Formation is not divided into members in the Timberville area, but Herbert and Young (1956) recognize two faunal zones, an upper Ceratopea zone and a lower Lecanospira zone, which correlate with the Bellefonte and Nittany members of the Beekmantown of Pennsylvania, respectively. The Beekmantown dolomite represents a portion of a long period of passive margin sedimentation from the late Precambrian to the Late Ordovician Taconic orogeny (Appold et al., 1995). A thick clastic wedge derived from the Taconic highlands, east of the present Appalachians, was deposited during the Late Ordovician to Early Silurian above the passive margin sedimentary sequence. The clastic wedge is represented by the Tuscarora and Shawangunk Formations. Rift-related metamorphosed sedimentary and volcanic rocks that are Late Proterozoic in age underlie the Beekmantown Formation. The Late Proterozoic rocks are underlain by Middle Proterozoic schists, gneisses, and intrusive rocks that have been metamorphosed (Appold et al., 1995). The Blountian epeirogeny of the Middle Ordovician produced a regionally extensive unconformity at the top of the Beekmantown Formation. This unconformity led to karst dissolution in the upper Beekmantown Formation. Karst dissolution led to increased fluid flow within the unit, which formed an aquifer in the carbonate sequence. High amounts of karstification led to highly porous breccia bodies, paleokarsts, within the unit, which allowed the growth of sulfide crystals (Appold et al., 1995). In the Timberville district, the upper Beekmantown Dolomite was interpreted to be a paleokarst breccia by Hoagland (1971). Due to the high permeability of karsts, sphalerite and other sulfides were mainly deposited in open spaces, with less than 15% of sulfide mineralization occurring as host rock replacement (Hoagland, 1971). Sulfide minerals are only observed in the upper 300 m of the Beekmantown Formation, which is consistent with a paleokarst origin (Herbert and Young, 1956). Gangue hydrothermal dolomite fills

the remaining space in the paleokarst network that is not occupied by host rock or sulfides. Sulfide mineralization occurs after brecciation of the host rock. Up to 10 different areas of sulfide mineralization have been identified in the Timberville district. Sphalerite is common to all locations, but pyrite, galena, fluorite, and chalcopyrite occurrences vary.

Objectives

Hypothesis

There is one hypothesis guiding this research:

• The salinity of fluid inclusions in sphalerite can be correlated to the chemical composition of the host sphalerite.

Test of Hypotheses

The hypothesis that is guiding this research will be tested by performing a series of analyses on samples from the Timberville Zn-Pb district, beginning with fluid inclusion microthermometric freezing point depression analyses. The salinity of the fluid inclusions, in wt% NaCl equivalent, will be calculated from the freezing point depression temperature by using the experimental data of Bodnar (1993). The freezing point depression of an aqueous liquid is a function of the number of atomic units that mix with a given number of water molecules in the aqueous solution. For solutes that comprise dominantly chloride salts, such as those in upper crustal fluids, the atomic mixing units are simple ions such as Cl⁻, Br⁻, $(SO_4)^{2-}$, $(CO_3)^{2-}$, H⁺, Na⁺, K⁺, Ca²⁺, Mg²⁺ and Sr²⁺, and their complexes. As these fluids vary in their salinity, they also vary in their depression of the freezing point. This suggests a convenient way to characterize different fluids by a simple measurement that is a function of total salinity, without the need to perform timeconsuming, sophisticated chemical analyses. The salinity of FIs is reported as wt. % NaCl equivalent, or the weight percent of NaCl that would produce the same freezing point depression as the aqueous solution of interest. Freezing point depression is a common phenomenon, found in eutectic systems, and results from the stabilization of the liquid by the entropy increase caused by molecular mixing in the liquid and the lack of such stabilization in the solid, which remains relatively pure; therefore, with increasing salinity, the liquid is stabilized relative to the solid, and its field of stability is increased. Fluid inclusion analyses were followed by electron probe microanalyzer (EPMA) analyses of the grain of sphalerite in which the fluid inclusions are contained, to determine the major and minor element chemistry of the grain. Cook et al. (2009) concluded that trace and minor elements in sphalerite can be accurately determined by using laser ablation inductively coupled plasma mass spectrometry (LA-ICPMS). Therefore, EPMA analyses will be followed by LA-ICPMS analyses on the same grains to determine the trace element chemistry of the grains in which the fluid inclusions of interest are hosted.

I have observed sphalerite grains that are visibly zoned, on a macroscopic level, within samples from the Bowers-Campbell mine. If the trace element compositions or

fluid inclusion properties differ between the core and the rim of zoned sphalerite grains, the observed variation could be indicative of a correlation between the chemical composition of the host sphalerite and the salinity of fluid inclusions. This potential variation may support the idea that the regional mineralization of sulfides may have occurred in multiple stages. A previous study has concluded that variations in the sulfur isotopic composition of sphalerite from samples collected from the Timberville district indicate that sulfide mineralization occurred in two stages (Appold et al., 1995). In that work, homogenization temperatures of fluid inclusions range from 110 °C to 165 °C for various samples from the Timberville district. Trace element compositions and fluid inclusion properties will be determined and compared to test the hypothesis that the salinity of fluid inclusions in sphalerite can be correlated to the chemical composition of the host sphalerite. The salinity data will be compared to trace element data of the host sphalerite to determine if the data are correlative. Variations in salinity may be related to variations in dilution of the ore fluid, which may produce variations in the trace element chemistry of the sphalerite.

Methods

Samples

During July 2012, ten samples were collected from tailings outside of the entrance to the Bowers-Campbell mine in Timberville, Virginia. An additional seven samples from the Bowers-Campbell mine were obtained from David Lipscomb of Afton, Virginia in October 2012. Samples from the Grove Hill road cut were also collected in October 2012, but it is interesting to note that I have not been able to find any sulfides in these samples, despite the reports of sphalerite being present (Herbert and Young, 1956). Five thin sections have been made from several of the initial samples collected from the Bowers-Campbell mine, and these samples were used for preliminary EPMA and LA-ICPMS analyses to demonstrate the feasibility of this project.

In December 2012 four samples were obtained from Stephen Kesler of University of Michigan. Two samples originate from the Bowers-Campbell mine (BC-4 and BC-11) (Figure 2), while the other two samples originate from the Weatherholz mine (TW-5 and TW-7.1). Appold et al. (1995) conducted sulfur isotope analyses and fluid inclusion

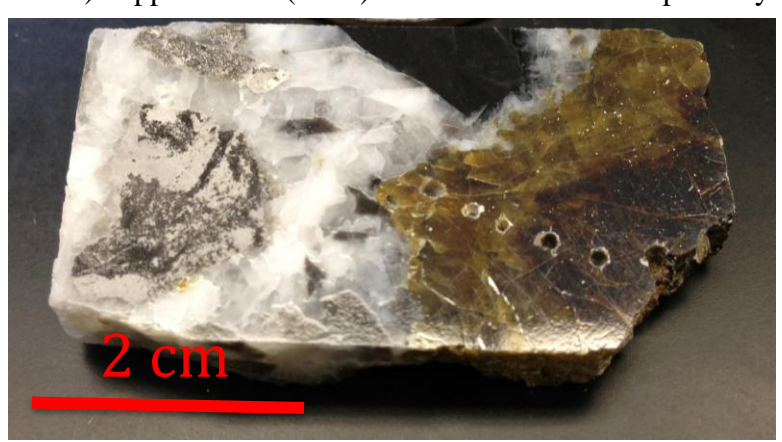


Figure 2: Sample BC-4 from the Bowers-Campbell mine.

microthermometry on each of the four samples, for which data is available. Some of these samples contain abundant grains of zoned sphalerite, for which there is previous data available, so these samples were used for the remaining research on this project from December 2012 until April 2013.

Sample Preparation

Sample analyses must be completed in a specific order so as to maximize the probability of matching fluid inclusion measurements with measurements of the composition of the host sphalerite; because finding an analyzable FI is quite difficult, FI microthermometry must be performed first. Then EPMA analyses are performed, followed by LA-ICPMS analyses. All samples were prepared as epoxy grain mounts prior to analysis. A total of 6 epoxy grain mounts were prepared, 3 of which contained grains of sphalerite from the Bowers-Campbell mine, and the remaining 3 mounts contained grains of sphalerite from the Weatherholz mine. Each epoxy grain mount contains approximately 20 grains of sphalerite.

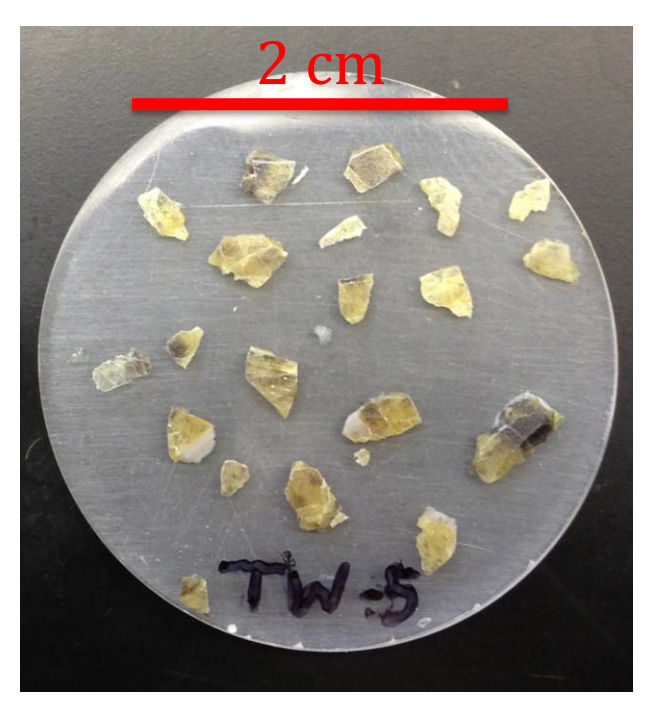


Figure 3: Grain mount of TW-5, with only one side polished.

Grains of sphalerite were selected and removed from samples. Those chosen to be mounted in epoxy range in size from 2-6 mm in length. These grains were set in an epoxy and allowed to cure for 24 hours. After curing, the epoxy grain mounts were hand polished to a thickness of ~100 µm (Figure 3). While polishing the surface of epoxy grain mounts, periodic checking of the thickness and surface conditions of the mount is necessary. To do this, I used an optical microscope and first focused on the surface of the epoxy mount closest to the microscope eyepiece. Then, I recorded the number on the focusing dial, moved the focus to the bottom of the epoxy grain mount, and recorded the number on the focusing dial again. The two numbers that I recorded give me the thickness of the epoxy grain mount. Each side of the epoxy grain mount was polished with a series of abrasives of which the finest was 0.3 µm grit. The grains in the epoxy grain mount were then inspected with a petrographic microscope to select fluid inclusions for analysis. The grain mount then underwent a series repolishing and inspection until ideal optical characteristics for the fluid inclusions present were reached. This process generally produces a polished grain mount 50-100 µm in thickness. In order for a fluid inclusion to have ideal optical properties, the fluid inclusion must be relatively close to the surface of the grain of sphalerite, causing the inclusion to exhibit a clear inner and outer boundary. An important aspect of the sample preparation process is getting a smooth even polish on each side of the grain mount. If a superior polish is not achieved, the fluid inclusion will not appear crisp in the microscope, and its features will be hard to distinguish.

After grain mounts are polished to the optimal thickness, individual grains are cut out of the surrounding epoxy so they can be mounted in the USGS-type gas-flow fluid

inclusion stage. Only one grain at a time can be mounted in the fluid inclusion stage, so grains with multiple suitable fluid inclusions are preferentially chosen for analysis.

Fluid Inclusion Microthermometry



Figure 4: USGS-type gas-flow fluid inclusion stage attached to an optical microscope in the Laboratory for Mineral Deposits Research at University of Maryland. Photo by Dr. Brian Tattitch.

Fluid inclusion microthermometric measurements were made on a USGS-type gas-flow fluid inclusion stage attached to an optical microscope in the Laboratory for Mineral Deposits Research (See Figure 4). The fluid inclusion stage allows heating and cooling of a sample in its sample chamber. For cooling experiments, cold nitrogen gas is introduced into the sample chamber, where a thermocouple is in contact with the sample. The thermocouple both holds the

sample in place and measures the temperature of the sample. Prior to cooling the sample, suitable fluid inclusions for microthermometry must be identified. Fluid inclusions that are suitable for analysis have a long dimension of no less than 10 micrometers, and are comprised of a vapor bubble and a liquid. After the sample is secured in the sample chamber with the thermocouple in place, the sample is brought to a temperature of -100 °C for 5 minutes with cold nitrogen gas. Next, the sample is slowly heated with a heating coil and phase changes are observed in the fluid inclusion. Changes that indicate melting in a fluid inclusion are the transition from sharp angular boundaries to rounded boundaries in a fluid inclusion in which such a change is observable, or Brownian motion of the vapor in a fluid inclusion in which Brownian motion was identified prior to cooling. Brownian motion is the random movement of a particle suspended in a fluid, due to bombardment from atoms in the fluid (Figure 5). For this study, only the method of observing Brownian motion was used because it is difficult to distinguish boundary shape changes in fluid inclusions of this size. Freezing point depression is determined by the observation of melting of a liquid phase in a fluid inclusion rather than freezing of the liquid phase because freezing requires nucleation, which yields more variable results. Measurements are then repeated for the same fluid inclusion seven times to obtain a mean freezing point depression.

The salinity of the fluid inclusions (FIs), in wt% NaCl equivalent, will be calculated from the freezing point depression temperature by using the experimental data of Bodnar (1993). The salinity of FIs is reported as wt. % NaCl equivalent because the actual composition of the fluid is unknown. For this study, the salinity of a fluid inclusion, in wt. % NaCl equivalent, is calculated by using the following equation from Bodnar (1993):

Equation 1: $Salinity = 1.78\theta - 0.0442\theta^2 + 0.000557\theta^3$ where θ is the depression of the freezing point in degrees Celsius. Equation 1 is based on experimental results (Hall et al., 1988).

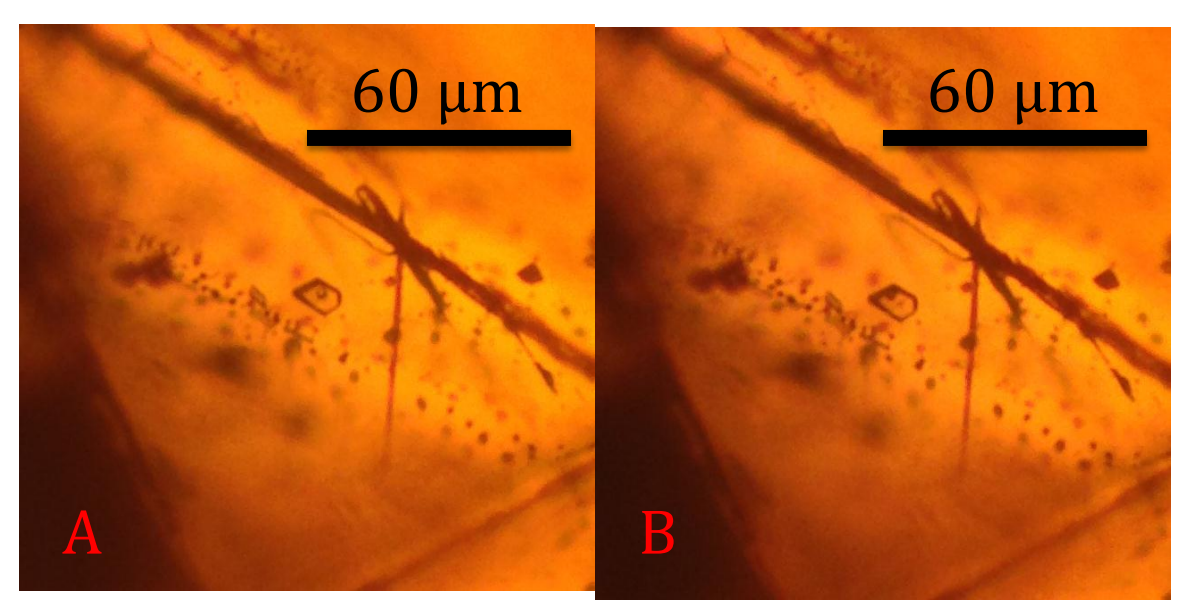


Figure 5: Brownian motion in a 10 μ m long fluid inclusion (center) in sphalerite. The vapor bubble at time 1 (A) is in a different position that it is at time 2 (B).

Fluid inclusion microthermometric measurements are performed first, so EPMA and LA-ICPMS analyses can target areas of a sample in which fluid inclusions, for which data are available, are present. Fluid inclusion microthermometry was performed on grains from samples BC-4 and BC-11 from the Bowers-Campbell mine, and samples TW-5 and TW-7.1 from the Weatherholz mine. BC-4, BC-11, TW-5, and TW-7.1 were all obtained from Stephen Kesler of University of Michigan. BC-4 and BC-11 contained zoned grains of sphalerite, for which samples from both the dark red core and the yellow rim were analyzed by fluid inclusion microthermometry. Samples TW-5 and TW-7.1 contained only grains of yellow sphalerite.

Mineral Analyses

Element Selection

Sphalerite is common to all locations with sulfide mineralization, thus the list of elements for analysis is based on chemical characteristics and past studies of sphalerite and formational brines of MVT deposits (Cook et al, 2009). A list of elements for analysis was created based on one criterion, and previous publications. The criterion for element selection is that the element must substitute into the sphalerite structure. Possible isomorphous substituents for zinc include: Fe²⁺, Cd²⁺, Mn²⁺, and Co²⁺. Se²⁻ can enter the sphalerite structure by a simple substitution for S²⁻ (Ye et al., 2011). Additionally, coupled substitution can occur, specifically that of Cu⁺ + In³⁺ for Zn²⁺ (Ye et al., 2011). This criterion adds Fe, Cd, Mn, Co, Se, Cu, In, Zn, and S to the element list.

The largest element list for analyses of sphalerite from a MVT deposit is provided by Ye et al. (2011). This criterion adds Ni, Ga, Ge, As, Ag, Sn, Sb, Te, Au, Tl, Pb, Bi, and U to the element list. Any additional elements that were analyzed for were added to the element list based on suggestions from Dr. Richard Ash for monitoring internal trends within grains of sphalerite.

Electron Probe Microanalyzer

A JEOL JXA-8900 electron probe microanalyzer was used for this project to determine major and minor element concentrations in minerals. Zn, Cd, S, Fe, In, Hg, and Cu concentrations were measured. Prior to analysis, a layer of carbon (200-300 Å) is applied to the surface of the samples using a thermal evaporator to make the surface more electrically conductive. Backscatter electron images are viewed to navigate throughout samples and are used in conjunction with optical scans in order to record the location of analyses. Semi-quantitative energy dispersive spectroscopy (EDS) analyses are run to estimate the composition of phases in thin section and to verify that the composition of certain phases are consistent with microscopic observations. Using the EDS results, areas of interest on the sample are defined and later analyzed by wavelength dispersive spectroscopy (WDS). WDS provides quantitative results for major and minor element concentrations. Measured values for reference materials are compared to known values to determine the accuracy of EPMA measurements. The external standard used for these analyses was Sphalerite-Nat for Zn and S, Chalcopyrite for Cu and Fe, and Cd for Cd. The areas of interest for EPMA analyses in this study are the areas immediately surrounding fluid inclusions that were analyzed by fluid inclusion microthermometry.

Laser Ablation Inductively Coupled Plasma Mass Spectrometry (LA-ICPMS)

Trace element compositions were measured by LA-ICPMS using a frequencyquintupled New Wave Nd-YAG 213 nm laser ablation unit coupled to a Thermo-Finnigan Element2 single-collector inductively coupled plasma mass spectrometer at the University of Maryland. Prior to tuning, the ICPMS was left running to warm-up for 120 minutes. The mass spectrometer is tuned prior to sample analysis to maximize the signal and minimize oxide production while ablating NIST SRM-610 (NIST-610). The external standard used for these analyses was NIST-610, an extensively characterized synthetic glass (Pearce et al., 1997). The spot size used in analyses was 100 µm for samples, and 55 μm for standards. Lines, rather than spots, were ablated on both standards and samples. Each set of analyses contains 20 total analyses, with the first and last two analyses being NIST-610, and analyses three, four, seventeen and eighteen being JB Sulphide, an inhouse standard reference material. Isotopes chosen for analysis by LA-ICPMS were ³³S, ⁴³Ca, ⁴⁷Ti, ⁴⁹Ti, ⁵⁵Mn, ⁵⁷Fe, ⁵⁹Co, ⁶¹Ni, ⁶²Ni, ⁶³Cu, ⁶⁵Cu, ⁶⁹Ga, ⁷¹Ga, ⁷³Ge, ⁷⁵As, ⁷⁷Se, ⁸²Se, ⁸⁵Rb, ⁸⁸Sr, ⁹⁵Mo, ⁹⁷Mo, ¹⁰⁷Ag, ¹¹¹Cd, ¹¹⁵In, ¹¹⁸Sn, ¹²¹Sb, ¹²⁵Te, ¹³⁷Ba, ¹⁹⁷Au, ²⁰⁵Tl, ²⁰⁸Pb, ²⁰⁹Bi, ²³²Th, and ²³⁸U. Isotopes were chosen based on the methodology described above for elements. Reported values for the concentration of an element, for which multiple isotopes were measured, is for the isotope with the lowest uncertainty associated with measurements. Iron is used as and internal standard. A background signal is collected for 20 seconds prior to each 50-second analysis. In between sample analyses, a washout period of two minutes was practiced to allow adequate time for cleaning of the sampleinjection tubing. Ion-intensities were measured in the low mass resolution mode.

LAMTRACE, a Lotus 123 macro-based spreadsheet package developed by Simon Jackson of Macquerie University, Australia, was used to process data from LA-ICPMS analyses (Jackson, 2001).

Error Analysis

The uncertainty on measurements from EPMA analyses is based on counting statistics. For standard x-ray counting statistics, the uncertainty can be calculated as follows: $1\sigma = \frac{\sqrt{n}}{n}$, where n is the number of counts measured for a given element in an analysis. For LA-ICPMS analyses, results are calculated from the measured values of standards and an internally standardized element, and the relative standard deviation is calculated by RSD = $\frac{standard\ deviation\ of\ sample\ array}{average\ of\ sample\ array}\ x\ 100$. The RSD defines the precision of the LA-ICPMS analyses. For fluid inclusion analyses, the RSD is calculated the same way as it is for LA-ICPMS analyses. There may be substantial error associated with assuming the contents of fluid inclusions to be only H₂O and NaCl, but determining the actual compositions of the fluid inclusion is beyond the scope of this project.

Results

Petrography

By using a petrographic microscope I was able to identify the minerals that are present in samples that were collected from the Bowers-Campbell mine, for which thin sections were made. In all thin sections I observed a dark fine-grained and a light coarse-grained dolomite, in BC12-1 and BC12-2 I observed sphalerite, and in BC12-5 I observed pyrite. In all thin sections the dominant mineral is dolomite, although the proportions of dark fine-grained dolomite, to light coarse-grained dolomite vary. All thin sections also appear to have irregular fractures present in the dark fine-grained dolomite and sphalerite that are filled with the light coarse-grained dolomite. In thin sections BC12-1 and BC12-2 I observed a light yellow sphalerite that is the second most dominant mineral. In many samples from the Bowers-Campbell mine, where sphalerite is present, I also observed a dark yellow-brown sphalerite that occurs in conjunction with the light yellow sphalerite. In BC12-1 the zoning of the sphalerite is apparent without magnification. The dark yellow-brown sphalerite makes up the core of the sphalerite grain, and the light yellow sphalerite makes up the rim of the grain (Figure 6). Zoned grains of sphalerite appear to be common in samples from the Bowers-Campbell mine.

Fluid Inclusion Microthermometry Results

Each fluid inclusion studied for this research exhibited Brownian motion of the vapor bubble that ceased upon freezing. All fluid inclusions that exhibited the cessation of Brownian motion were about 10 μm in diameter. Seven fluid inclusions in yellowbrown sphalerite from the Bowers Campbell mine were determined to have mean freezing point depressions that range from 7.3 \pm 0.91 °C to 9.9 \pm 0.69 °C at the 2 σ level. The mean freezing point depression of fluid inclusions in the set of samples from yellow-

brown sphalerite was 8.3 °C, with a 2σ standard deviation of 1.7 °C for the set of data. A statistically significant difference in values for fluid inclusion freezing point depression from samples BC-4 and BC-11 was not observed. Four fluid inclusions in the lighter yellow sphalerite from the Bowers Campbell mine were determined to have mean freezing point depressions that range from 19.3 ± 2.1 °C to 21.2 ± 3.7 °C at the 2σ level. The mean freezing point depression of fluid inclusions in the set of samples from yellow sphalerite from the Bowers-Campbell mine was 20.1 °C, with a 2σ standard deviation of 1.7 °C for the set of data. All of the samples from the Weatherholz mine only contained a light yellow sphalerite, and a statistically significant difference in values for fluid inclusion freezing point depression from samples TW-5 and TW-7.1 was not observed. Seven fluid inclusions in the lighter yellow sphalerite from the Weatherholz mine were determined to have mean freezing point depressions that range from 18.2 ± 1.1 °C to 20.7 ± 1.3 °C at the 2σ level. The mean freezing point depression of fluid inclusions in the set of samples from yellow sphalerite from the Bowers-Campbell mine was 19.8 °C, with a 2σ standard deviation of 1.8 °C for the set of data.

Fluid inclusion salinities that correspond to the measured freezing point depression are calculated using Equation 1, based on data from Bodnar (1993). The freezing point depressions measured from the fluid inclusions in yellow-brown sphalerite from the Bowers Campbell mine correspond to salinities, in wt. % NaCl equivalent, that range from 10.9 ± 4.5 to 13.8 ± 2.9 at the 2σ level. The mean salinity of fluid inclusions in the set of samples from yellow-brown sphalerite was 12.0 wt. % NaCl equivalent, with a 2σ standard deviation of 1.9 wt. % NaCl equivalent for the set of data. The freezing point depressions measured from the fluid inclusions in yellow sphalerite from the Bowers Campbell mine correspond to salinities, in wt. % NaCl equivalent, that range from 21.9 ± 2.9 to 23.2 ± 4.9 at the 2σ level. The mean salinity of fluid inclusions in the set of samples from yellow-brown sphalerite was 22.4 wt. % NaCl equivalent, with a 2 σ standard deviation of 1.1 wt. % NaCl equivalent for the set of data. Finally, the freezing point depressions measured from the fluid inclusions in yellow sphalerite from the Weatherholz mine correspond to salinities, in wt. % NaCl equivalent, that range from 21.1 ± 3.2 to 22.9 ± 3.4 at the 2σ level. The mean salinity of fluid inclusions in the set of samples from yellow-brown sphalerite was 22.2 wt. % NaCl equivalent, with a 2 σ standard deviation of 1.2 wt. % NaCl equivalent for the set of data.

Electron Probe Microanalyzer Results

WDS analyses of thin section BC12-1 from the Bowers-Campbell mine conducted on the EPMA revealed that the average Fe content of the core of a zoned grain of sphalerite was greater than that of the rim by an order of magnitude (Figure 6 & Figure 7). A standard line scan was performed on sample BC12-1 from the rim (A) to the core (B)

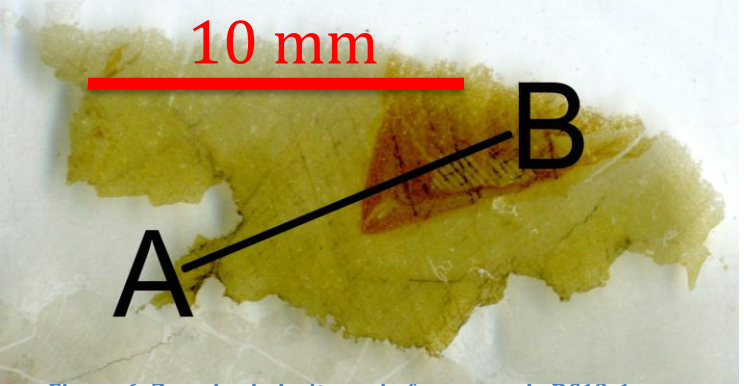


Figure 6: Zoned sphalerite grain from sample BC12-1.

of the large sphalerite grain (Figure 6). Note that the Fe concentration begins to rise shortly after half way through the WDS scan on the zoned sphalerite grain. The rise in Fe indicates the transition from the light yellow rim of the sphalerite grain to the dark yellow-brown core (Figure 7).

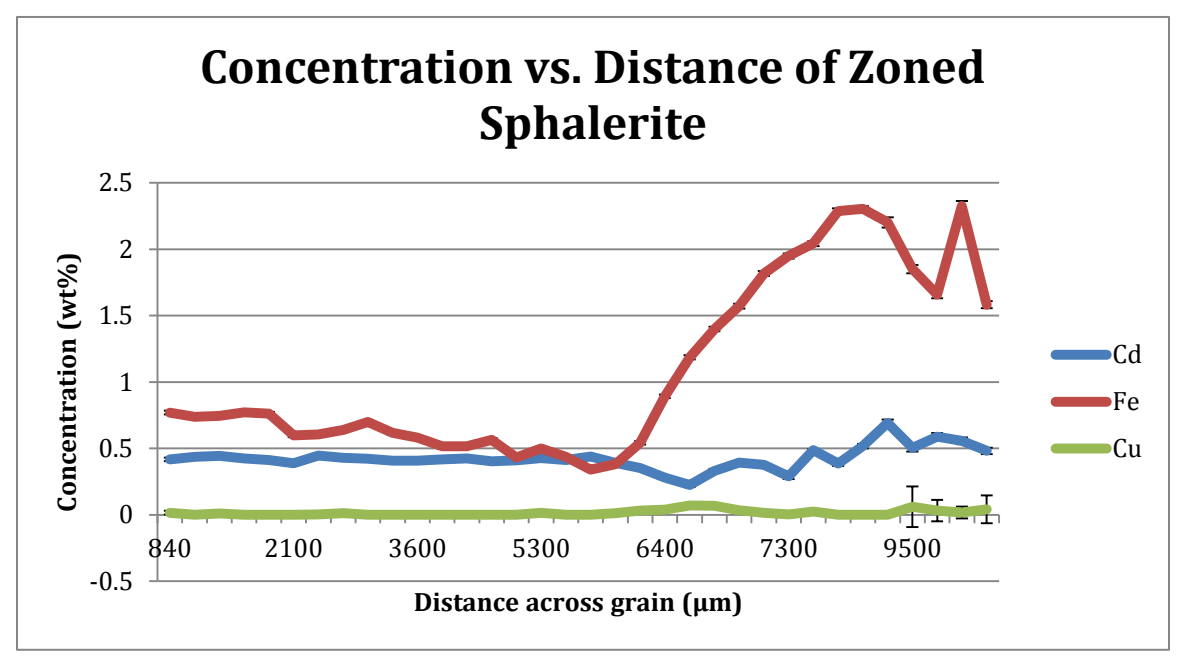


Figure 7: Concentration of Cd, Fe, and Cu vs. distance for a WDS scan of the zoned sphalerite grain in BC12-1. Note the increase in Fe concentration about half way through the scan.

The Fe content of the dark yellow-brown sphalerite grains from samples BC-4 and BC-11, measured by EPMA WDS analyses, ranges from 1.25 ± 0.19 wt. % to 2.36 ± 1.03 wt. % at the 2σ level. The mean Fe content of the dark yellow-brown sphalerite in the set of samples from BC-4 and BC-11 was 1.6 wt. %, with a 2σ standard deviation of 0.6 wt. % for the set of data. The Fe content of the lighter yellow sphalerite grains from samples BC-4 and BC-11 ranges from 0.06 ± 0.02 wt. % to 0.3 ± 0.06 wt. % at the 2σ level. The mean Fe content of the light yellow sphalerite in the set of samples from BC-4, BC-11, TW-5, and TW-7.1 was 0.15 wt. %, with a 2σ standard deviation of 0.03 wt. % for the set of data. Elements other than iron did not show significant variation in concentration on the weight % level between the yellow-brown sphalerite and the yellow sphalerite.

Laser Ablation Inductively Coupled Plasma Mass Spectrometry Results

Trace element concentration data were collected using LA-ICPMS on grains of sphalerite from samples BC-4, BC-11, TW-5, and TW-7.1. Results are grouped into trace element concentrations for Fe-poor, or light yellow sphalerite, and Fe-rich, or dark yellow-brown sphalerite. Gallium is the only element, of those measured, found to vary between high-Fe and low-Fe sphalerite outside of the 2σ variation within each data set (Figure 8, 9, 10, 11). The mean Ga content of the dark yellow-brown, Fe-rich sphalerite grains from samples BC-4 and BC-11, is 39.3 ± 46.8 ppm at the 2σ level. In contrast, the mean Ga content of the light yellow, Fe-poor sphalerite in the set of samples from BC-4, BC-11, TW-5, and TW-7.1 is 385.3 ± 216.1 ppm at the 2σ level.

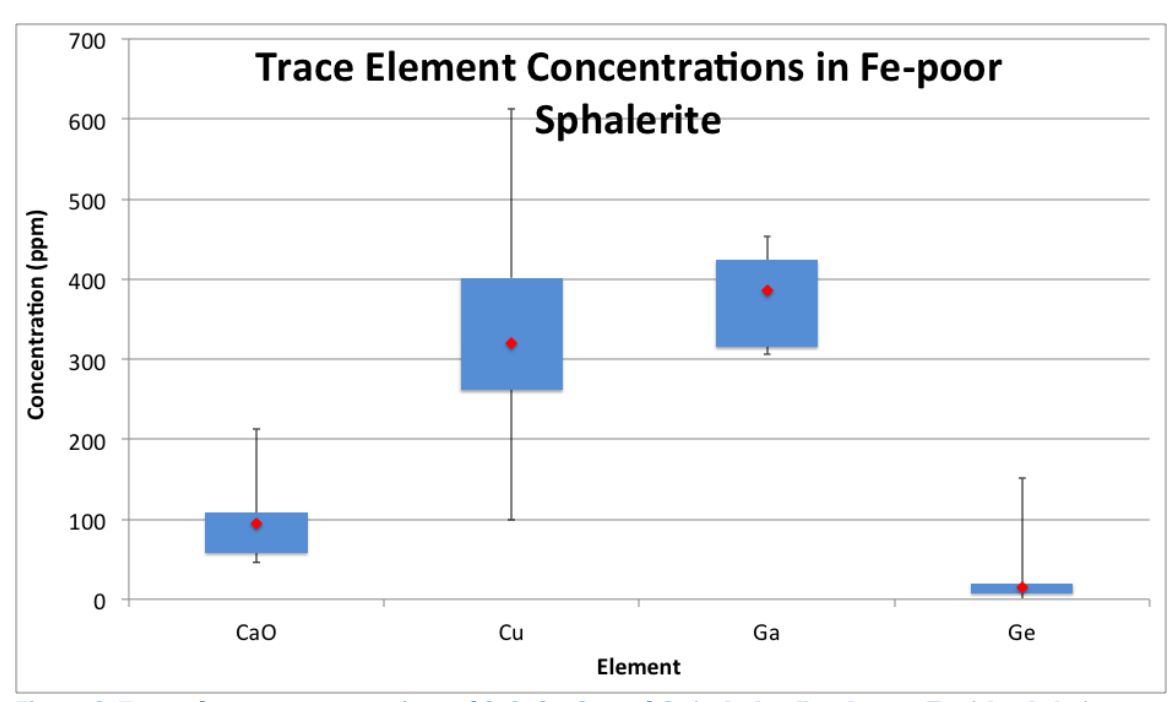


Figure 8: Trace element concentrations of CaO, Cu, Ga, and Ge in dark yellow-brown, Fe-rich sphalerite grains from samples BC-4 and BC-11.

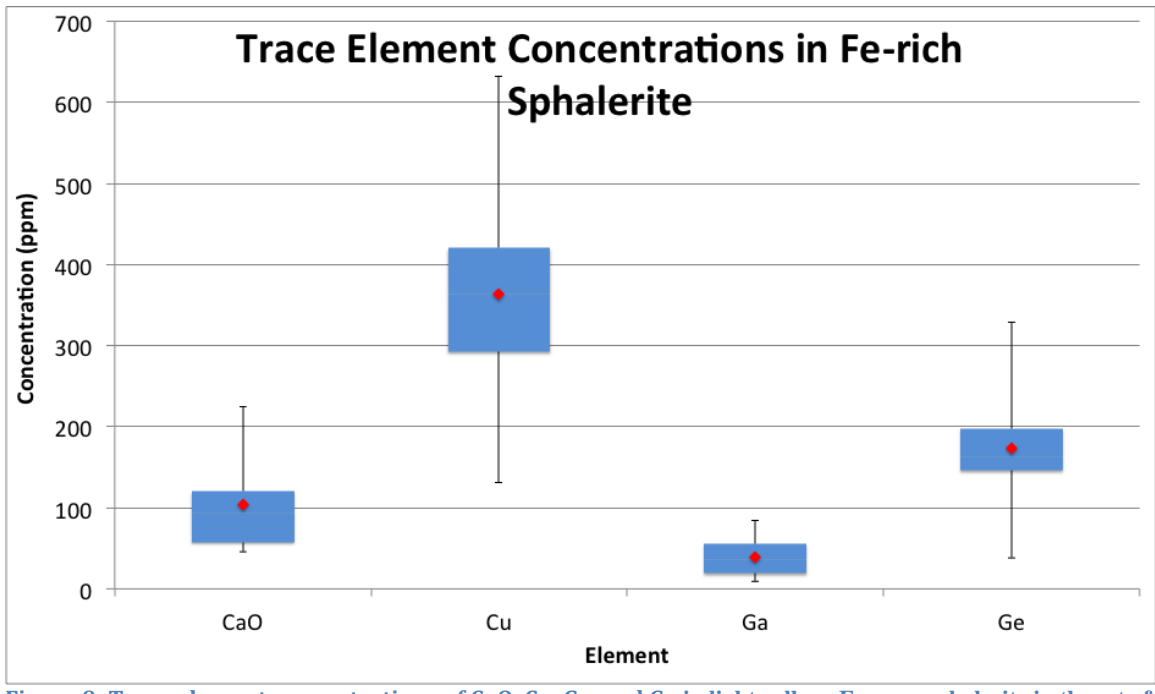


Figure 9: Trace element concentrations of CaO, Cu, Ga, and Ge in light yellow, Fe-poor sphalerite in the set of samples from BC-4, BC-11, TW-5, and TW-7.1

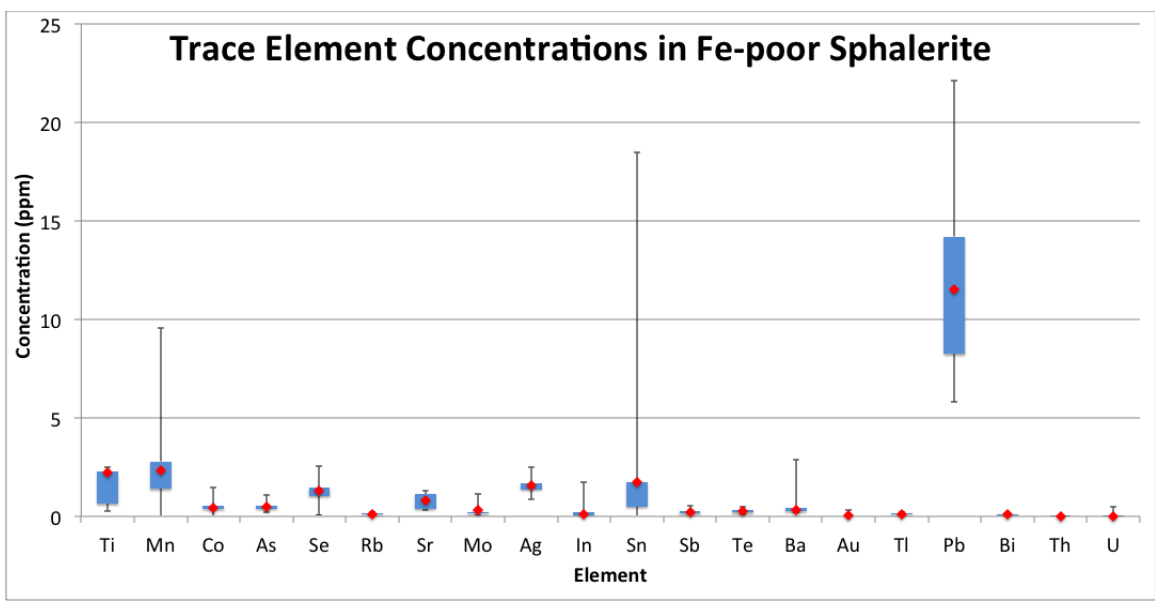


Figure 10: Trace element concentrations of Ti, Mn, Co, As, Se, Rb, Sr, Mo, Ag, In, Sn, Sb, Te, Ba, Au, Tl, Pb, Bi, Th, and U in dark yellow-brown, Fe-rich sphalerite grains from samples BC-4 and BC-11.

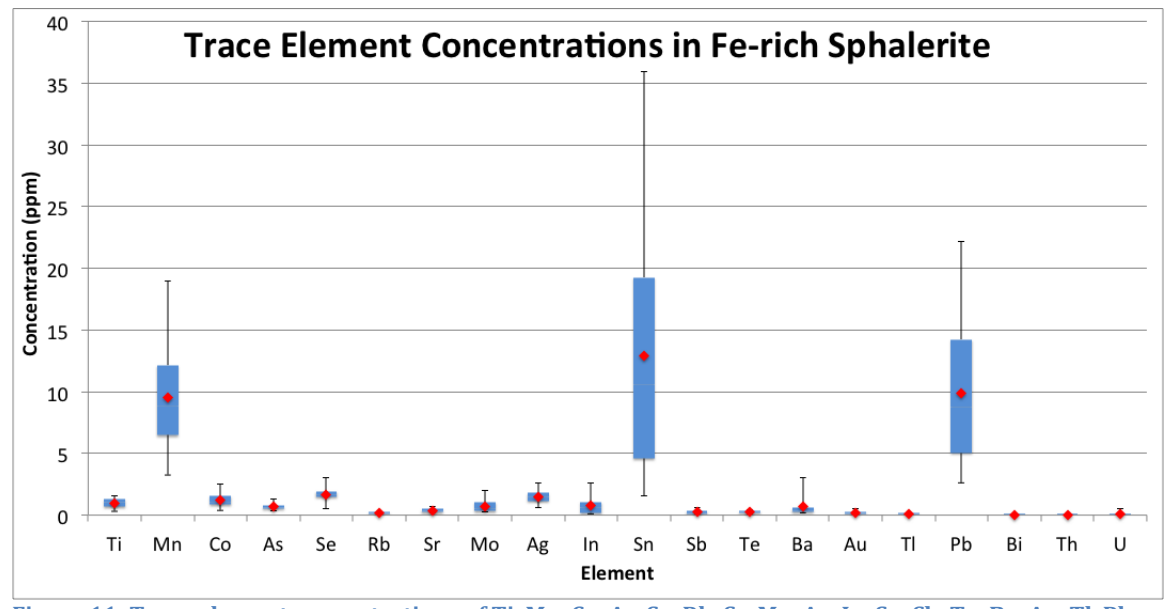


Figure 11: Trace element concentrations of Ti, Mn, Co, As, Se, Rb, Sr, Mo, Ag, In, Sn, Sb, Te, Ba, Au, Tl, Pb, Bi, Th, and U in light yellow, Fe-poor sphalerite in the set of samples from BC-4, BC-11, TW-5, and TW-7.1

Discussion

Chemical Variation in Sphalerite

The concentration of iron in sphalerite varies on a weight percent level, and is reflected in the color of the crystal, thus it is useful to compare the iron concentration of a grain of sphalerite to the salinity of fluid inclusions in the grain. Figure 12 shows that the two different types of sphalerite are distinct based on salinity and Fe concentration, at the 2σ margin of error. Ga has also been determined to vary with salinity (Figures 8 & 9), but

Fe varies on a weight percent level, so Fe was chosen for Figure 12 to show a more distinct correlation.

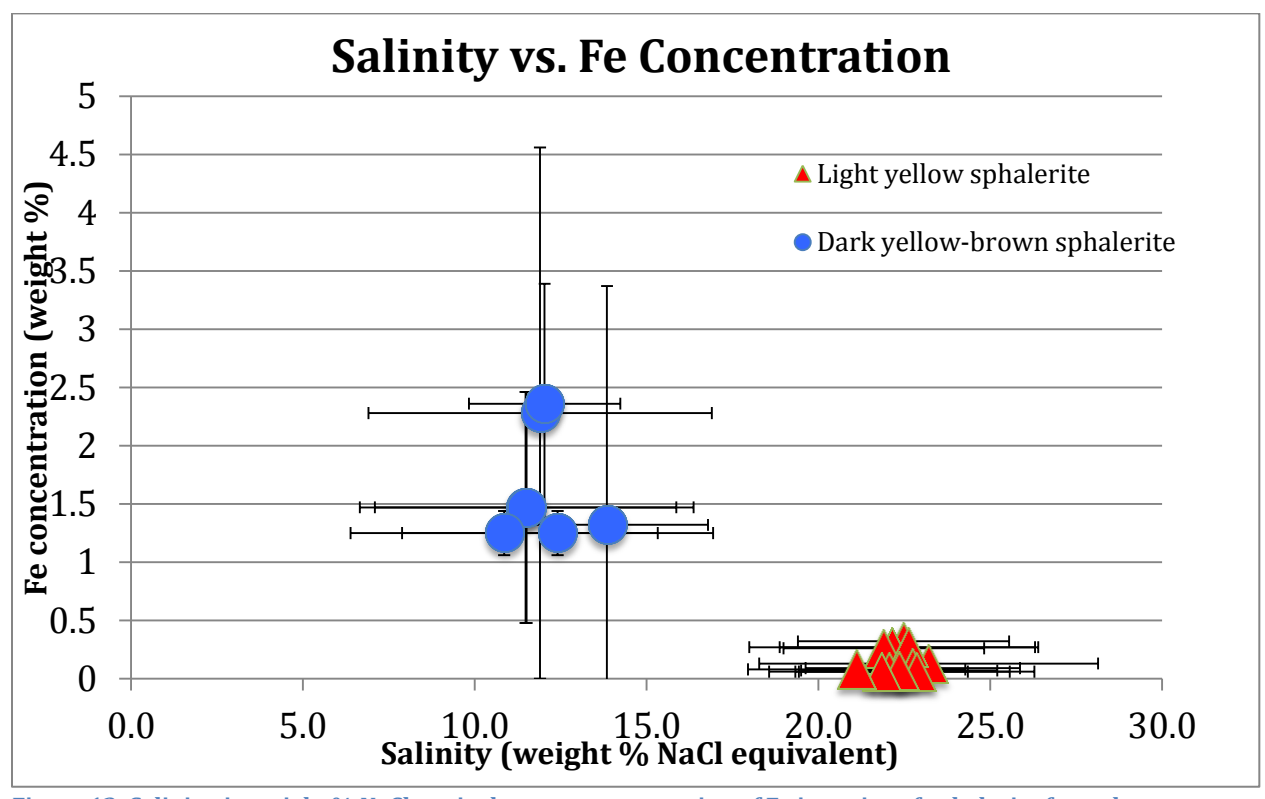


Figure 12: Salinity, in weight % NaCl equivalent, vs. concentration of Fe in grains of sphalerite from the Timberville Zn-Pb district. The error bars represent the standard deviation within a set of analyses.

Fluid Inclusion Freezing Point Depressions in Sphalerite

The range of freezing point depression temperatures found in fluid inclusions of samples with light yellow sphalerite is consistent with the temperature range of 24 °C to 12 °C reported by Appold et al. (1995). Appold et al. (1995) did not analyze fluid inclusion in dark yellow-brown sphalerite from the Bowers-Campbell mine, which have been found to have a lower freezing point depression than fluid inclusions in yellow sphalerite (Figure 12). It is worth noting that Appold et al. (1995) also found a subset of fluid inclusions with freezing point depressions of 42 °C to 29 °C, which were not observed in this study.

Implications For Formational Fluids

Fluid inclusion salinity and chemical composition in grains of sphalerite from the Timberville Zn-Pb district are correlative. This observation may suggest that two formational fluids, from which sphalerite formed, experienced different degrees of mixing during the time periods that light and dark sphalerite were formed. The mixing of solutions is considered to play an important role in the precipitation of sulfides in MVT deposits (Corbella et al., 2004). The data presented in this paper supports the idea that the mixing of formational fluids in MVT deposits affects properties of the precipitated sulfides (Shelton et al., 1992, Kesler, 1996). The correlation of fluid inclusion salinity

and chemical composition of sphalerite also might suggest that the chemistry of the formational fluids changed between the deposition of the two types of sphalerite, possibly from the introduction of an additional fluid to the system.

Anderson (1975) suggested that the dominant formational fluids for sulfide precipitation are metal-bearing brines and sulfide-rich solutions (Equation 2).

Equation 2: $H_2S(aq) + Zn^{2+} = ZnS(s) + 2H^+$

The salinity and composition of the two dominant formational fluids may vary, thus the degree of mixing of these fluids will yield fluids with varying salinities and sphalerite with varying compositions, consistent with the observations of this study (Corbella et al., 2004). Additionally, the relative proportion of dissolved cations in subsurface fluids varies with changes in the total ionic charge of the aqueous solution, reflected by chlorinity and salinity (Hanor, 2001). Hanor (2001) determined that reactive transport should occur in rock-buffered systems in any porous medium where there is a chlorinity gradient, even where molecular diffusion is the dominant solute transport mechanism and local chemical equilibrium or fixed cation—chloride relations are maintained throughout. Therefore, it is likely that the high-Fe and low-Fe sphalerite in a single location were precipitated at different times due to a change in the composition of the fluid from which the sphalerite was precipitating, likely due to fluid mixing.

Suggestions For Future Work

An observed variation in Fe and Ga that is correlated to fluid inclusion salinity warrants further investigation in zoned sphalerite from other MVT deposits. A further investigation will reveal whether the correlation between fluid inclusion salinity and chemistry is local or global.

Conclusions

The concentrations of iron and gallium in sphalerite grains from the Bowers-Campbell mine and the Weatherholz mine in the Timberville Zn-Pb district are correlative with the salinity of fluid inclusions in the host sphalerite. Sphalerite with a higher concentration of iron, and therefore a darker color, hosts fluid inclusions with a lower freezing point depression than sphalerite with a lower Fe concentration. The relationship of the concentration of gallium with respect to salinity is conversely proportional to that of iron. This finding supports the conclusion that regional sulfide mineralization occurred in multiple stages, suggested by Appold et al. (1995). This finding also may suggest that two formational fluids, from which sphalerite formed, experienced different degrees of mixing during the time periods that light and dark sphalerite were formed.

Acknowledgements

I thank my advisors, Dr. Philip Candela, Dr. Philip Piccoli, and Dr. William McDonough for their guidance and expertise in their respective fields. I would also like

to thank Dr. Brian Tattitch for teaching me the basics of fluid inclusion microthermometry. I would like to thank Dr. Richard Ash for his advice and assistance with completing laser ablation analyses on the ICP-MS, and for his advice with respect to data processing. I would like to thank Dr. Martin Appold and Dr. Stephen Kesler for providing me with samples from the Timberville Zn-Pb district. Finally, I would like to thank the faculty, staff, and students of the Department of Geology that asked me probing questions and allowed me to ask them questions.

Bibliography

- Alldrick D., and Sangster D. "Mississippi Valley-Type (MVT) Pb-Zn Mineral Deposit Profile." Yukon Geological Survey (2005)
- Anderson GM. "Precipitation of Mississippi Valley-type ores." Economic Geology (1975) 70:937–942
- Appold, M. S., S. E. Kesler, and J. C. Alt. "Sulfur Isotope and Fluid Inclusion Constraints on the Genesis of Mississippi Valley-type Mineralization in the Central Appalachians." Economic Geology 90.4 (1995): 902-19.
- Bodnar, R. "Revised Equation and Table for Determining the Freezing Point Depression of H2O-Nacl Solutions." Geochimica Et Cosmochimica Acta 57.3 (1993): 683-84.
- Cook, Nigel J., Cristiana L. Ciobanu, Allan Pring, William Skinner, Masaaki Shimizu, Leonid Danyushevsky, Bernhardt Saini-Eidukat, and Frank Melcher. "Trace and Minor Elements in Sphalerite: A LA-ICPMS Study." Geochimica Et Cosmochimica Acta 73.16 (2009): 4761-791.
- Corbella, Merce, Ayora, Carlos, Cardellach, Esteve. "Hydrothermal mixing, carbonate dissolution and sulfide precipitation in Mississippi Valley-type deposits." Mineralium Deposita 39 (2004): 344-357
- Hanor JS. "Reactive transport involving rock-buffered fluids of varying salinity." Geochimica Cosmochimica Acta (2001) 65:3721–3732
- Herbert, Paul, Jr., and Robert S. Young. "Sulfide Mineralization in the Shenandoah Valley of Virginia." Department of Conservation and Development, Virginia Division of Geology 70 (1956)
- Hoagland, A. D. "Appalachian Strata-bound Deposits; Their Essential Features, Genesis and the Exploration Problem." Economic Geology 66.5 (1971): 805-10.
- Hõy, T., "Irish-Type Carbonate-Hosted Zn-Pb." B.C. Geological Survey Deposit Type, (1996)

- Jackson, S. E. "LAMTRACE user's manual." School of Earth Sciences, Macquarie University, Sydney, Australia (2001).
- Kesler SE "Appalachian Mississippi Valley-type deposits: paleoaquifers and brine provinces. In: Sangster DF (ed.) Carbonate-hosted lead-zinc deposits." Soc Econ Geol Spec Publ (1996) 4: 29–57
- Kesler, S. E., M. S. Appold, G. L. Cumming, and D. Krstic. "Lead Isotope Geochemistry of Mississippi Valley-type Mineralization in the Central Appalachians." Economic Geology 89.7 (1994): 1492-500.
- Kesler, Stephen E., and Ben A. van der Pluijm. "Timing of Mississippi Valley-type Mineralization: Relation to Appalachian Orogenic Events." Geology 18.11 (1990): 1115.
- Leach, David L., and E. Lanier Rowan. "Genetic Link between Ouachita Foldbelt Tectonism and the Mississippi Valley–type Lead-zinc Deposits of the Ozarks." Geology 14.11 (1986): 931.
- Leach, David L., Donald F. Sangster, Karen D. Kelley, Ross R. Large, Grant Garven, Cameron R. Allen, Jens Gutzmer, and Steve Walters. "Sediment-Hosted Lead-Zinc Deposits: A Global Perspective." Economic Geology 100th Aniversary (2005): 561-607.
- Leach, David L., Ryan D. Taylor, David L. Fey, Sharon F. Diehl, and Richard W. Saltus. "A Deposit Model for Mississippi Valley-Type Lead-Zinc Ores." USGS Scientific Investigations Report A 5070 (2010)
- MacIntyre, D., "Sedimentary Exhalative (SEDEX) Zn-Pb-Ag, Mineral Deposit Profiles." Yukon Geological Survey (2005)
- Marie, James St., Stephen E. Kesler, and Cameron R. Allen. "Origin of Iron-rich Mississippi Valley-type Deposits." Geology 29.1 (2001): 59.
- Nesse, William D. Introduction to Mineralogy. New York: Oxford UP, 2000.
- Pearce, Nicholas J.G., William T. Perkins, John A. Westgate, Michael P. Gorton, Simon E. Jackson, Clive R. Neal, and Simon P. Chenery. "A Compilation of New and Published Major and Trace Element Data for NIST SRM 610 and NIST SRM 612 Glass Reference Materials." Geostandards and Geoanalytical Research 21.1 (1997): 115-44.
- Shelton KL, Bauer RM, Gregg JM. "Fluid-inclusion studies of regionally extensive epigenetic dolomites, Bonneterre Dolomite (Cambrian), southeast Missouri: evidence of multiple fluids during dolomitization and lead-zinc mineralization." Geol. Soc. Am. Bull. (1992) 104:675–683

- Sweet, P.C., Good, R.S., Lovett, J.A., Campbell, E.V.M., Wilkes, G.P., and Meyers, L.L.. "Copper, lead, and zinc resources in Virginia: Virginia Division of Mineral Resources Publication 93" (1989): 185
- Wenz, Zachary John. "Geochemistry and Origins of Mississippi Valley Type Mineralizing Fluids of the Ozark Plateau." PhD. Dissertation (2011)
- Wilkinson, J.J., "Fluid inclusions in hydrothermal ore deposits." Lithos 55 (2001): 229-272
- Ye, Lin, Nigel J. Cook, Cristiana L. Ciobanu, Liu Yuping, Zhang Qian, Liu Tiegeng, Gao Wei, Yang Yulong, and Leonid Danyushevskiy. "Trace and Minor Elements in Sphalerite from Base Metal Deposits in South China: A LA-ICPMS Study." Ore Geology Reviews 39 (2011): 188-217.

Appendix A

Major and minor element concentrations in sample BC12-1 from EPMA analyses. Values in weight percent

No.	Zn		Cd	s	Fe	In	Hg	Cu	Total	Comment
	1	65.39	0.22	33.01	1.29	0.00	0.05	0.06	100.03	0-1
	2	64.33	0.34	33.24	1.10	0.00	0.07	0.00	99.08	0-2
	3	65.84	0.40	33.36	2.03	0.00	0.00	0.01	101.64	0-3
	4	64.84	0.34	32.61	1.22	0.00	0.02	0.00	99.03	1-1
	5	64.68	0.27	32.75	1.35	0.00	0.09	0.01	99.15	1-2
	6	65.54	0.35	32.31	1.18	0.00	0.20	0.00	99.58	1-3
	7	66.15	0.40	33.74	1.65	0.00	0.08	0.00	102.02	5-1
	8	64.06	0.27	33.76	3.59	0.00	0.01	0.04	101.73	5-2
	9	66.23	0.41	33.43	1.59	0.00	0.15	0.00	101.80	5-3
	10	42.76	0.29	31.86	2.12	0.00	0.00	0.04	77.07	5-4
	11	43.41	0.37	32.34	2.01	0.00	0.12	0.01	78.25	5-5
	12	43.71	0.08	32.61	2.96	0.00	0.00	0.05	79.41	5-6
	13	66.46	0.28	33.04	0.72	0.00	0.02	0.02	100.54	5-7
	14	65.66	0.33	33.10	2.50	0.00	0.00	0.05	101.64	5-8
	15	66.81	0.24	32.96	0.74	0.00	0.00	0.02	100.76	5-9
	16	65.61	1.14	32.63	0.29	0.00	0.22	0.00	99.89	11-1
	17	65.76	1.13	33.01	0.27	0.00	0.13	0.00	100.30	11-2
	18	66.97	1.06	33.23	0.25	0.00	0.08	0.00	101.57	11-3
	19	64.91	0.31	33.62	0.08	0.00	0.00	0.07	99.00	11-4
	20	64.84	0.31	34.52	0.11	0.00	0.21	0.07	100.06	11-5
	21	67.82	0.35	32.57	0.09	0.00	0.09	0.08	101.01	11-6
	22	65.47	0.30	32.49	0.05	0.00	0.10	0.05	98.45	12-1
	23	63.20	0.23	32.91	0.06	0.00	0.00	0.03	96.42	12-2
	24	60.34	0.25	32.83	0.07	0.00	0.02	0.03	93.54	12-3
	25	67.15	0.23	33.20	0.06	0.00	0.02	0.03	100.69	12-4
	26	68.50	0.26	32.46	0.05	0.00	0.03	0.01	101.30	12-5
	27	66.69	0.22	32.47	0.06	0.00	0.11	0.02	99.57	12-6
	28	64.68	0.35	31.87	0.07	0.00	0.05	0.04	97.06	13-1
	29	66.10	0.48	31.49	0.07	0.00	0.16	0.00	98.29	13-2
	30	66.94	0.40	32.03	0.07	0.00	0.00	0.00	99.43	13-3
	31	66.49	0.25	32.23	0.06	0.00	0.10	0.02	99.16	13-4
	32	68.24	0.28	32.74	0.04	0.00	0.11	0.01	101.42	13-5
	33	69.11	0.26	32.75	0.06	0.00	0.09	0.04	102.31	13-6
	34	64.22	0.25	32.92	0.06	0.00	0.00	0.00	97.45	13-7
	35	66.40	0.23	33.09	0.09	0.00	0.05	0.02	99.88	13-8
	36	65.71	0.41	32.94	0.08	0.00	0.02	0.00	99.15	13-9

Relative uncertainties for sample BC12-1 from EPMA analyses.

Zn	Cd	S	Fe	In		Hg	Cu	Comment
1	0.7	5.21	0.27	1.26	100	140.25999	16.49	0-1
2	0.71	3.63	0.27	1.39	100	97.8	100	0-2
3	0.7	3.05	0.27	0.94	100	100	106.56	0-3
4	0.73	3.7	0.27	1.31	100	370.41	100	1-1
5	0.73	4.44	0.27	1.22	100	80.78	90.92	1-2
6	0.73	3.48	0.27	1.35	100	33.66	100	1-3
7	0.72	3.14	0.27	1.09	100	92.5	100	5-1
8	0.73	4.39	0.27	0.68	100	793.48999	29.86	5-2
9	0.72	3.08	0.27	1.11	100	46.05	100	5-3
10	0.91	4.26	0.27	0.95	100	100	27.54	5-4
11	0.9	3.45	0.27	0.99	100	61.42	93.44	5-5
12	0.9	14.5	0.27	0.77	100	100	21.77	5-6
13	0.72	4.17	0.27	1.91	100	481.79001	49.79	5-7
14	0.72	3.69	0.27	0.84	100	100	23.49	5-8
15	0.71	4.85	0.27	1.92	100	100	53.1	5-9
16	0.69	1.39	0.27	3.86	100	31.65	100	11-1
17	0.69	1.38	0.27	4.18	100	55.6	100	11-2
18	0.68	1.46	0.27	4.57	100	92.61	100	11-3
19	0.63	3.79	0.27	12.57	100	100	15.11	11-4
20	0.68	3.78	0.27	9.13	100	34.16	14.8	11-5
21	0.68	3.47	0.28	11.06	100	75.86	13.61	11-6
22	0.76	4.1	0.27	20.81	702.81	69.95	23.42	12-1
23	0.78	5.23	0.27	17.65	100	100	41.71	12-2
24	0.8	4.75	0.27	13.42	100	341.82001	38.95	12-3
25	0.69	4.99	0.27	15.01	100	440.20001	41.24	12-4
26	0.68	4.4	0.28	21.66	100	218.2	140.42999	12-5
27	0.7	5.32	0.28	16.41	100	64.1	50.3	12-6
28	0.72	3.56	0.28	13.6	100	151.39	27.04	13-1
29	0.71	2.81	0.28	14.29	100	44.78	100	13-2
30	0.71	3.12	0.28	15	100	100	300.78	13-3
31	0.7	4.68	0.28	15.9	100	67.11	60.42	13-4
32	0.7	4.23	0.28	23.13	100	68.85	99.5	13-5
33	0.7	4.57	0.27	16.11	100	80.34	27.48	13-6
34	0.72	4.66	0.27	16.03	100		1340.27002	13-7
35	0.71	5.18	0.27	11.09	100	142.73	44.68	13-8
36	0.72	3.11	0.27	13.6	100	484.70999	100	13-9

Appendix B

LA-ICPMS data for sample BC12-1. nd = below detection limit.

									41380	04/15/13								
Filter = <3 X LLD	CaO	Ti	Ti	Mn	Fe	Co	Ni	Ni	Cu	Cu	Ga	Ga	Ge	As	Se	Se	Rb	Sr
Isotopic mass	43	47	49	55	57	59	61	62	63	65	69	71	73	75	77	82	85	88
	ppm	ppm	ppm	ppm	ppm	ppm	ppm	ppm	ppm	ppm	ppm	ppm	ppm	ppm	ppm	ppm	ppm	ppm
Run detection limit	7.9	0.086	0.12	0.046	3.0	0.019	3.8	3.7	0.20	0.10	0.020	0.024	0.17	0.042	0.087	0.45	0.012	0.0071
NIST610	84595	459	454	494	458	422	475	<1975.06	440	474	465	455	474	359	148	144	454	530
NIST610	79820	409	414	476	458	388	442	nd	420	386	401	411	420	291	128	132	397	501
JB SULPHIDE	1785	20	18	1397	97000	nd	629944	741867	6299	5411	0.61	nd	nd	nd	nd	nd	0.94	1.6
JB SULPHIDE	3799	78	18	1235	97000	nd	588678	768312	5365	4645	0.96	nd	nd	nd	nd	nd	0.53	2.2
0-1	nd	nd	4.0	6.3	12855	1.7	nd	nd	402	340	52	58	164	0.56	1.8	nd	0.14	0.30
0-2	nd	nd	2.5	7.3	10955	0.88	nd	nd	296	258	26	28	145	0.41	1.5	nd	0.12	0.62
0-3	nd	nd	7.2	10	20329	2.5	nd	nd	731	632	76	84	328	0.94	3.0	nd	0.24	0.71
1-1 1-2	nd 58	nd	5.0 3.5	5.5	12239 13549	2.1 1.5	nd	nd	464 540	412 477	26 15	28 15	203 251	0.54 0.42	1.6	nd	0.15 0.12	0.15 0.19
1-3	146	nd 1.1	3.4	7.1 6.6	11761	1.0	nd nd	nd	320	283	34	36	134	0.42	1.5 1.6	nd nd	0.12	0.19
5-1	46	0.31	3.4	9.4	16484	0.71	nd	nd nd	388	340	16	18	153	0.56	1.5	nd	0.13	0.00
5-2	112	nd	7.0	19	35902	1.7	nd	nd	634	571	55	58	251	1.1	2.7	nd	0.13	0.25
5-3	225	1.5	4.2	8.8	15882	0.94	nd	nd	330	302	15	17	147	0.53	1.2	nd	0.13	0.33
5-4	nd	nd	4.6	13	21208	0.85	nd	nd	410	376	8.6	9.2	192	0.79	1.7	nd	0.15	0.14
5-5	58	nd	5.5	11	20099	1.1	nd	nd	466	429	34	37	190	0.73	2.1	nd	0.24	0.37
5-6	nd	nd	5.4	16	29555	1.1	22	12	415	371	20	20	155	1.3	2.0	nd	0.31	0.42
5-7	109	nd	1.3	3.2	7172	0.53	nd	nd	143	130	74	80	38	0.34	0.52	nd	0.045	0.25
5-8	nd	nd	7.0	16	25049	1.1	nd	nd	396	364	43	47	178	0.69	nd	nd	0.20	0.49
5-9	78	nd	2.2	3.5	7364	0.38	nd	nd	181	168	50	52	67	0.70	0.56	nd	0.053	0.21
11-1	362	nd	12	8.8	2885	0.97	nd	1445	2686	2446	2018	2249	76	2.0	4.1	nd	0.40	5.0
11-2	225	nd	11	5.9	2689	0.90	nd	nd	2395	2189	1743	1966	65	1.4	3.3	nd	0.30	4.0
11-3	142	1.3	10	5.5	2467	0.89	nd	nd	2052	1904	1406	1750	57	1.3	nd	nd	0.32	2.4
11-4	88	0.35	3.4	4.2	795	0.19	nd	nd	450	425	399	432	5.3	nd	1.3	nd	0.094	2.4
11-5	106	nd	4.0	5.5	1080	nd	nd	nd	592	552	595	638	8.8	0.46	1.9	nd	nd	1.9
11-6	79	nd	4.0	4.1	918	0.27	nd	nd	621	573	502	573	7.7	0.51	1.5	nd	nd	1.8
12-1	42	nd	3.0	1.5	475	0.38	nd	nd	314	298	261	282	14	0.39	0.89	nd	0.093	0.18
12-2	47	nd	4.2	2.7	560	0.40	31	nd	394	364	317	362	18	0.56	1.2	nd	0.11	0.56
12-3	nd	0.52	5.1	2.7	725	0.63	nd	nd	520	475	467	497	26	0.64	1.4	nd	0.14	0.28
12-4	58	nd	2.7	1.4	637	0.64	nd	nd	nd	402	342	364	21	0.37	nd	nd	0.11	0.65
12-5	nd	nd	2.1	1.6	456	0.42	nd	44	358	313	266	274	19	0.44	0.89	nd	nd	0.38
12-6	43	nd	3.5	1.1	590	0.31	8.3	nd	229	216	307	325	8.6	0.36	1.1	nd	0.093	0.43
13-1	nd	8.4	3.5	3.5	716	0.45	nd	67	351	331	474	510	9.1	0.66	1.2	nd	0.13	0.43
13-2	118	nd	5.0	2.7	693	0.47	nd	nd	336	297	376	400	18	0.63	1.3	nd	nd	0.29
13-3	105	nd	3.6	1.7	662	0.44	nd	60 76	269	251	301	321	17	0.42	1.2	nd	0.11	0.55
13-4 13-5	190 91	nd	5.0 3.0	1.0 0.65	615 442	0.59 0.38	nd nd	76 11	389 307	357 291	293 223	313 243	25 21	0.49 0.30	1.0 1.0	nd	0.12	1.8 0.43
13-6	nd	nd 0.83	3.8	0.65	618	0.56	nd 1.9	nd	448	400	317	243 341	29	0.56	1.0	nd nd	nd 0.12	0.43
13-7	nd	3.4	o.o nd	nd	620	nd	nd	254	123	93	275	290	4.5	nd	1.9	nd	nd	0.23
13-8	157	1.2	6.0	1.8	874	0.51	nd	nd	62	63	372	394	3.5	nd	nd	nd	0.14	1.1
13-9	108	0.76	4.6	2.8	769	0.51	nd	nd	70	70	352	375	3.1	0.57	1.7	nd	0.14	1.1
JB SULPHIDE	1068	28	55	1371	97000	nd	3301457	1256875	6666	5934	nd	nd	nd	nd	nd	nd	1.5	1.4
JB SULPHIDE	354	5.8	11	1290	97000	nd	1692397	1378576	6073	5876	nd	nd	nd	nd	nd	nd	0.74	0.79
NIST610	88786	467	472	534	458	445	nd	nd	465	467	476	473	488	357	151	153	464	562
NIST610	75654	401	424	436	458	365	nd	nd	395	393	390	393	406	293	125	123	387	nd
nbs 610 reference2 JB-sulfide	82199	434	434	485 1125	458 97000	405	459 566000	459 566000	430 2160	430 2160	433	433	447	325	138	138	426	516

Filter = <3 X LLD Isotopic mass	Mo 95 ppm	Mo 97 ppm	Ag 107 ppm	Cd 111 ppm	In 115 ppm	Sn 118 ppm	Sb 121 ppm	Te 125 ppm	Ba 137 ppm	Au 197 ppm	TI 205 ppm	Pb 208 ppm	Bi 209 ppm	Th 232 ppm	U 238 ppm	Peak secs	Abltn yield
Run detection limit	0.0083	0.011	0.0065	0.54	0.0035	0.022	0.0074	0.026	0.021	0.017	0.0015	0.0077	0.0043	0.0011	0.00092		
NIST610	451	446	293	296	480	467	430	331	463	26	64	445	414	467	472	30	92%
NIST610	383	388	209	246	392	393	362	273	441	21	55	407	362	448	451	40	122%
JB SULPHIDE	2.7	3.8	16	0.43	nd	2.6	1.0	0.17	3.7	3.3	nd	120	nd	nd	nd	30	117%
JB SULPHIDE	2.6	3.5	6.3	nd	nd 0.45	2.5	0.85	0.090	7.3	2.7	0.029	117	nd	nd 0.0031	0.076	34	130%
0-1 0-2	0.30 0.24	0.42 0.41	1.1 0.94	5485 3708	0.15 0.18	2.4 1.7	0.12 nd	0.28 nd	0.18 0.32	0.24 nd	0.025 0.054	3.0 2.6	nd 0.026	0.0031	0.0039 0.00	36 27	612% 906%
0-3	0.24	0.41	2.1	8034	0.16	1.7	0.20	0.48	0.32	0.27	0.054	4.5	0.026 nd	0.00	0.00	36	419%
1-1	0.36	0.39	1.5	3866	0.36	8.6	0.20	0.48	0.47	0.27	0.004	3.3	nd	0.0042	0.0048	35	690%
1-2	0.24	0.32	1.4	3045	0.58	6.6	0.079	0.20	0.31	0.095	0.10	5.6	nd	0.0029	0.22	32	841%
1-3	0.40	0.48	1.3	3233	1.3	15	0.075	0.21	2.6	0.099	0.14	15	nd	0.0025	0.0035	26	969%
5-1	0.25	0.34	1.2	3618	0.89	24	0.24	0.23	0.22	0.51	0.045	9.3	0.031	0.00	0.0040	37	923%
5-2	1.2	1.6	2.6	7495	2.6	20	0.62	nd	0.62	0.33	0.075	19	0.059	0.00	0.021	36	532%
5-3	0.43	0.44	1.6	3628	0.79	11	0.40	0.22	0.84	nd	0.027	8.7	0.022	0.0022	0.0053	32	1068%
5-4	0.52	0.72	1.5	4720	0.11	2.6	0.35	0.24	nd	0.11	0.048	13	nd	0.00	0.0061	38	773%
5-5	0.50	0.70	1.9	5839	0.79	28	0.25	0.30	3.1	nd	0.074	13	0.036	0.00	0.0043	41	705%
5-6	1.6	1.8	1.7	7429	0.18	6.9	0.62	0.42	0.50	0.20	0.078	22	0.046	0.00	0.028	38	643%
5-7	2.0	2.2	0.62	1678	1.4	11	0.10	nd	0.18	0.12	0.039	6.2	0.012	0.0014	0.061	32	2395%
5-8	1.2	1.3	2.2	5880	1.3	36	0.31	0.25	0.41	0.17	0.12	16	0.037	0.0047	0.026	16	629%
5-9	1.0	1.2	0.80	1651	0.57	19	0.13	0.12	0.30	0.18	0.041	6.7	0.074	0.0019	0.50	19	1852%
11-1	4.6	0.54	3.4	11382	63	8.3	0.64	0.77	0.80	nd	1.2	90	nd	0.0094	0.00	26	271%
11-2	0.49	0.61	3.1	10816	39	3.3	0.61	nd	1.2	nd	1.0	81	nd	0.0045	0.00	30	327%
11-3	0.35	0.69	2.7	8873	21	2.2	0.51	0.53	0.75	nd	0.89	76	nd	0.00	0.00	28	390%
11-4	0.11	0.17	1.1	3184	23	4.0	0.37	0.21	0.48	nd	0.081	14	nd	0.00	0.00	28	1102%
11-5	0.24	0.25	1.6	3976	41	5.7	0.44	0.24	0.43	nd	0.12	19	nd	0.0028	0.0037	32	795%
11-6	0.27	0.17	1.6	3374	38	5.6	0.31	0.22	0.38	nd	0.11	15	nd	0.00	0.00	38	884%
12-1	0.16	0.18	1.4	2738	0.098	1.6	0.17	0.21	0.22	0.054	0.091	7.2	0.033	0.00	0.0050	34	1078%
12-2	0.18	0.20	1.4	3183	0.16	1.6	0.19	0.20	0.26	nd	0.13	8.2	nd	0.0019	0.0029	34	893%
12-3	0.23	0.31	1.9	3862	0.20	1.4	0.28	0.37	0.21	nd	0.18	13	0.050	0.0036	0.0029	27	704%
12-4	0.18	0.21	1.4	3039	0.23	0.86	0.18	0.19	0.41	nd	0.18	9.3	nd	0.030	0.00	38	834%
12-5	0.13	0.14	0.99	1907	0.20	2.9	0.15	nd	0.21	nd	0.15	7.2	nd 0.27	0.0022	0.17	20 32	1122%
12-6 13-1	2.7 0.15	0.28 0.33	1.2 1.6	3649	0.086 0.30	0.25 1.8	0.16 0.45	nd	0.32 0.29	nd	0.064 0.083	7.1 14	0.27	0.0041 0.0026	0.00 0.0022	32 17	846%
13-1	0.15 0.18	0.33	1.6	4598 3851	0.30	1.8	0.45	nd nd	0.29	nd nd	0.083	16	nd nd	0.0026	0.0022	17	676% 708%
13-3	0.16	0.25	1.7	3244	0.20	0.96	0.27	0.25	0.34	nd	0.16	12	0.091	0.0035	0.0012	34	708% 842%
13-4	0.13	0.21	1.7	3268	0.20	0.90	0.19	0.25	0.34	nd	0.13	14	0.031	0.0018	0.00	41	733%
13-5	0.14	0.22	1.7	2275	0.034	0.41	0.17	0.30	0.18	nd	0.10	9.5	nd	0.0026	0.0016	41	1080%
13-6	0.12	0.19	1.9	3101	0.017	0.26	0.10	0.36	0.39	nd	0.16	14	nd	0.0020	0.00	18	748%
13-7	nd	nd	1.4	4019	0.042	0.33	nd	0.00	nd	nd	nd	5.6	nd	0.00	0.00	0.00	728%
13-8	0.23	0.25	2.5	6453	0.13	0.75	0.24	0.49	0.51	nd	0.028	14	0.042	0.00	0.0035	43	547%
13-9	0.18	0.25	1.5	6125	0.25	1.1	0.17	0.39	0.32	nd	0.027	8.2	0.17	0.00	0.0025	43	581%
JB SULPHIDE	4.3	3.5	25	nd	nd	4.0	1.4	0.23	6.0	2.6	nd	224	0.25	0.024	0.13	32	142%
JB SULPHIDE	3.0	2.9	9.9	nd	nd	2.0	0.73	nd	4.0	2.6	nd	193	nd	0.0071	0.14	21	136%
NIST610	453	454	278	305	484	471	434	336	489	26	68	476	435	494	509	41	98%
NIST610	381	380	224	237	388	389	358	268	469	21	59	376	341	421	414	44	88%
nbs 610	417	417	251	271	436	430	396	302	452	24	59	426	388	457	462		
reference2 JB-sulfide	2.5	2.5								0.056		8.0					

Appendix C

Honor Code:

"I pledge on my honor that I have not given or received any unauthorized assistance or plagiarized on this assignment."